Biosensors and Bioelectronics 126 (2019) 418–424

Contents lists available at ScienceDirect

Biosensors and Bioelectronics

journal homepage: www.elsevier.com/locate/bios

Development of cardiac troponin-I biosensor based on boron nitride quantum dots including molecularly imprinted polymer

Mehmet Lütfi Yola[a,*], Necip Atar[b]

[a] Iskenderun Technical University, Faculty of Engineering and Natural Sciences, Department of Biomedical Engineering, Hatay, Turkey
[b] Pamukkale University, Faculty of Engineering, Department of Chemical Engineering, Denizli, Turkey

ARTICLE INFO

Keywords:
Molecular imprinted biosensor
Cardiac Troponin-I
Boron nitride quantum dots
Plasma

ABSTRACT

The cardiac Troponin-I (cTnI) is one of the subunits of cardiac troponin complexes and a pivotal biochemical marker of acute myocardial infarction (AMI). Due to its myocardial specificity, cTnI is widely used for the diagnosis of AMI diseases. In this study, a novel imprinted biosensor approach based on boron nitride quantum dots (BNQDs) was presented for cTnI detection in plasma samples. Various characterization methods such as scanning electron microscope (SEM), transmission electron microscope (TEM), x-ray diffraction (XRD), cyclic voltammetry (CV) and electrochemical impedance spectroscopy (EIS) were used for all characterizations of nanomaterials. After the characterization analysis, cTnI imprinted electrode was developed in the presence of 100.0 mM pyrrole containing 25.0 mM cTnI. After that, the analytical studies of cTnI in plasma samples were performed by using cTnI imprinted biosensor. The results of the study have revealed that 0.01–5.00 ng mL^{-1} and 0.0005 ng mL^{-1} were found as the linearity range and the detection limit (LOD). Moreover, the selectivity of cTnI imprinted glassy carbon electrode (GCE) was investigated for plasma sample analysis in the presence of other nonspecific and specific proteins including cardiac myoglobin (MYG), bovine serum albumin (BSA) and cardiac troponin T (cTnT), respectively. Furthermore, the prepared biosensor was examined in terms of stability, repeatability, reproducibility and reusability. Finally, the imprinted biosensor was applied to the plasma samples having high recovery.

1. Introduction

It is known that AMI is one of the factors causing death in the world (Friess and Stark, 2009; Iwanaga and Miyazaki, 2010). cTnI is a biochemical marker of AMI due to its well specificity and sensitivity for acute myocardial damage and inhibitor protein of the troponine-tropomyosin complex. The molecular weight of cTnI is known to be 29 kDa (Fredericks et al., 1998; Liu et al., 2016) and its concentration in the human body is lower than 0.4 ng mL^{-1}. Provided that this amount is found to be higher than 2.0 ng mL^{-1}, then the potential risk may be stated for cardiovascular diseases (Boriani et al., 2000). When the literature was reviewed, the analytical methods such as enzyme-linked immunosorbent assay (ELISA) (de Antonio et al., 2013), chemiluminescent immunoassays (Cho et al., 2009) and radioimmunoassay (Apple et al., 1997) have been developed in terms of instant analysis of cTnI. Monitoring myocardial infarction by means of easy, rapid, sensitive and selective methods plays a crucial role for the potential risks of cardiac diseases. Accordingly, sensitive and cost-efficient analytic methods are immediately required for the instant analysis of cTnI.

Hexagonal boron nitride nanosheets are known as 2D materials and can be used for sensor applications, catalysis, bioimaging and drug delivery (Weng et al., 2014). The large band-gap property of 2D-hBN nanosheets makes them transparent in visible and IR regions. In addition, due to their surface area and conductivity, they have significant electrochemical sensor applications (Atar and Yola, 2018; Khan et al., 2016). Moreover, 2D-hBN nanosheets were examined in order to load metal nanoparticles as well (Ide et al., 2014). On the other hand, BNQDs may be obtained by reducing the size of the layered hexagonal boron nitride nanosheets. The dispersibility and fluorescence properties of these nanosheets are accepted at a very good level due to their quantum confinement and edge effects (Hongling et al., 2015; Marc et al., 2014). Moreover, they can be used in biological and optoelectronic implementations (Lei et al., 2015; Mengli et al., 2017).

After completing the formation of BNQDs, cTnI imprinted electrodes were prepared on BNQDs modified GCE (BNQDs/GCE) by means of molecular imprinting technology. The technology is a polymerization method around analyte molecule and forms the specific cavities for target molecules on polymeric network (Beytur et al., 2018; Yola and

* Corresponding author.
E-mail address: mlutfi.yola@iste.edu.tr (M.L. Yola).

https://doi.org/10.1016/j.bios.2018.11.016
Received 9 June 2018; Received in revised form 5 November 2018; Accepted 12 November 2018
Available online 13 November 2018
0956-5663/

Atar, 2017a). The molecularly imprinted electrochemical biosensors for cTnI detection were formed by the synergistic interactions between cTnI imprinted polymers and BNQDs. Therefore, the specific cavities for cTnI molecule were created for selective analysis in the mixed matrix medium.

2. Experimental

2.1. Materials

The materials used in this study were as follows: cTnI, MYG, BSA and cTnT (Sigma-Aldrich, USA), Pyrrole (Merck, Germany), boron nitride powders (Merck, Germany), potassium ferricyanide ($K_3Fe(CN)_6$, Sigma–Aldrich, USA). In addition, standard solutions of cTnI, MYG, BSA and cTnT (1.0 mM) were prepared in a phosphate buffer solution (PBS) (0.1 M, pH 7.0).

2.2. Instrumentation

The electrochemical performances and differential pulse voltammograms (DPVs) were measured by IviumStat (U.S). X-ray diffraction measurements were performed by Rikagu Miniflex X-ray diffractometer. The XPS images were obtained by PHI 5000 Versa Probe (Japan/USA) and SEM images were obtained by ZEISS EVO 50 analytic microscope (Germany).

2.3. Preparation of BNQDs

The powder of bulk boron nitride (100.0 mg) was dispersed in IPA (50.0 mL) in order to prepare two-dimensional (2D) hexagonal boron nitride (2D-hBN). The dispersion was heated at the temperature of 50 °C for 24 h under stirring. Afterwards, the dispersion was subjected to ultrasonication for 20 h. Then, the obtained supernatant was centrifugated at 15,000 rpm for 10 min. Finally, the precipitate was washed with acetone several times and dried at 60 °C overnight to obtain 2D-hBN nanosheets (Atar and Yola, 2018). After 2D-hBN nanosheets were degassed with N_2 for 30 min in order to remove the oxygen, the dispersions were decanted into autoclave under solvothermal conditions of 180 °C for 10 h. Then, they were cooled to room temperature. After the centrifugation at 10,000 rpm, the supernatant was collected as BNQDs (Mengli et al., 2017).

2.4. Electrode preparation

The glassy carbon electrodes were cleaned according to our study (Yola and Atar, 2017b). 10 µL suspensions of 2D-hBN and BNQDs were dropped on the clean electrode surface and the solvent was removed under an infrared heat lamp. All electrodes were stored in a sealed box without fluctuations of temperature and pressure. In addition, the DPVs were obtained in insulation cabinet in terms of avoiding temperature and pressure fluctuation affecting the sensor response.

2.5. Preparation of cTnI imprinted sensor and cTnI removal from electrode surface

The procedure of cTnI imprinted BNQDs electrode (MIP/BNQDs/GCE) was shown on Scheme 1. After the development of BNQDs/GCE, 100.0 mM pyrrole containing 25.0 mM cTnI (Supporting electrolyte: 0.1 M, pH 7.0 PBS) was prepared in voltammetric cell. 10 cycles were performed for the formation of imprinting polymer on CV (Scan rate: 100 mV s^{-1}). The imprinting selectivity was analyzed by imprinted electrode based on BNQDs/GCE without cTnI (NIP/BNQDs/GCE). 1.0 M NaCl was used as desorption solution for eliminating electrostatic interactions between monomer and analyte molecules. Then cTnI imprinted electrode was swinged in bath (25 mL NaCl solution, 200 rpm) at room temperature. After 15 min, the electrode was dried with nitrogen gas (Yola et al., 2017). Ag/AgCl/KCl(sat) and Pt wire were used as the reference and counter electrode in this study.

2.6. Sample preparation

In this study, MIP/BNQDs/GCE was applied to plasma samples to present the application of developed electrode. The cTnI free plasma samples were obtained from Blood Bank of Hacettepe University Hospital in TURKEY.

For the experiments of recovery, four different plasma samples were prepared (Plasma sample1, Plasma sample2, Plasma sample3 and Plasma sample4). The contents of solutions were listed below:

(1) 0.83 ng mL^{-1} cTnI, 0.83 ng mL^{-1} MYG, 0.83 ng mL^{-1} BSA and 0.83 ng mL^{-1} cTnT
(2) 0.83 + 0.05 ng mL^{-1} cTnI, 0.83 ng mL^{-1} MYG, 0.83 ng mL^{-1} BSA and 0.83 ng mL^{-1} cTnT
(3) 0.83 + 0.10 ng mL^{-1} cTnI, 0.83 ng mL^{-1} MYG, 0.83 ng mL^{-1} BSA and 0.83 ng mL^{-1} cTnT
(4) 0.83 + 0.50 ng mL^{-1} cTnI, 0.83 ng mL^{-1} MYG, 0.83 ng mL^{-1} BSA and 0.83 ng mL^{-1} cTnT

The standard cTnI, MYG, BSA and cTnT solutions (0.83 ng mL^{-1}) were firstly added into the cTnI free plasma samples (Plasma sample1). After that, 0.05, 0.10 and 0.50 ng mL^{-1} standard cTnI solutions were added into the solutions one by one, respectively (Plasma sample2, Plasma sample3 and Plasma sample4). After each addition of cTnI solutions, plasma samples were spiked: 1:2 mL methanol was added to an aliquot of 0.4 mL plasma sample in a 2.0 mL plastic centrifuge tube. After that, the centrifugation at 20,000 rpm was performed for 15 min. The upper clear layer solution was diluted with 0.1 M PBS, pH 7.0 for analysis. The voltammograms were recorded in the potential range from 0.0 V to + 1.0 V by cTnI imprinted electrode. The informed consent will be obtained for improved experimentation with real human subjects in future.

3. Results and discussion

3.1. Nanostructures characterization

Fig. 1A demonstrates XRD patterns of bulk boron nitride (curve a) and 2D-hBN nanosheets (curve b). XRD pattern of bulk boron nitride reveals the characteristic diffraction peaks corresponding to (100), (101), (102) planes (Hassan et al., 2012). The characteristic diffraction peaks of bulk boron nitride disappeared on XRD pattern of 2D-hBN nanosheets. However, (002) plane of boron nitride remained intact (Li et al., 2011). SEM image (Fig. 1B) of boron nitride confirms its bulk structure. In the bulk structure, irregular morphology, agglomeration and varying dimensions of boron nitride were observed. The 2D-hBN nanosheets were obtained after ultrasonication of bulk boron nitride. Fig. 1C suggested the formation of 2D-hBN nanosheets. The particle thickness decreased with the lateral sizes of 2D-hBN nanosheets in comparison with bulk boron nitride. Fig. 1D revealed TEM image of BNQDs, indicating that the obtained BNQDs were well dispersed with uniform lateral sizes. The average lateral sizes were found to be 4.4 ± 0.6 nm (Fig. 1E). In addition, we have examined the formation of MIP and NIP surfaces. The intensive cTnI imprinted polymer layer was obtained on SEM analysis (Fig. 1F). When SEM image of NIP surface was investigated, the less porous structure was seen in comparison with MIP surface (Fig. 1G).

3.2. CV and EIS characterizations of bare GCE, 2D-hBN/GCE and BNQDs/GCE

According to CV results (Fig. 2A), the peaks of 1.0 mM $[Fe(CN)_6]^{3-}$ with 150 mV of peak potential difference (ΔEp) were observed at bare

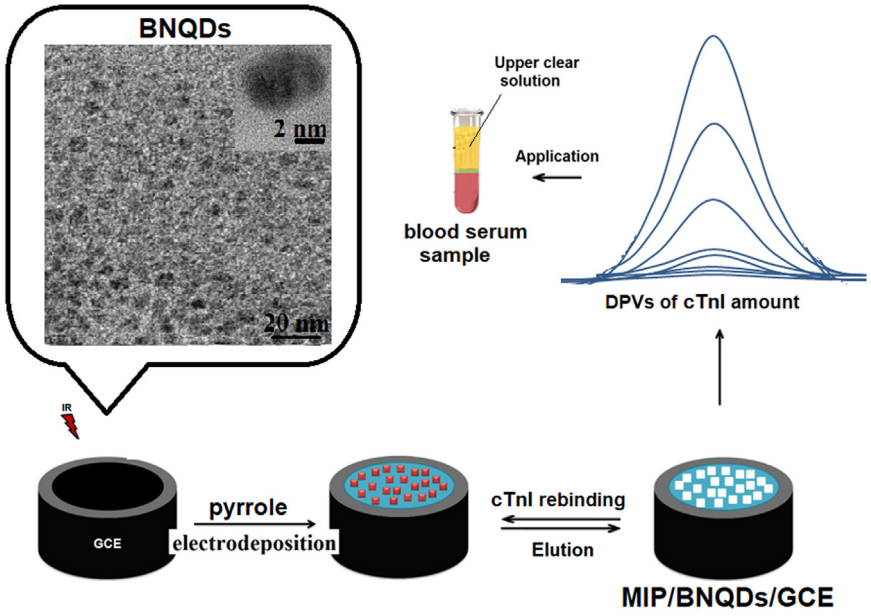

Scheme 1. The procedure of MIP/BNQDs/GCE.

GCE (curve a). After modification of 2D-hBN on bare GCE, ΔEp decreased to 100 mV with an obvious increase in the peak signals (curve b). Due to large surface area and thermal conductivity of 2D-hBN nanosheets, the increase of current signals was noted (Khan et al., 2016). The higher current increase was seen when BNQDs modified GCE was used (ΔEp = 50 mV) (curve c). It was stated that it had an impact on sensor signals resulted from the layered BNQDs with the smaller size. In addition, excellent conductivity and optical properties and good dispersibility, biocompatibility of BNQDs were endowed due to the quantum confinement, edge effects and defect centers (Mengli et al., 2017). Moreover, it could be noted that BNQDs had a similar structure to the graphite. Thus, the enhanced mechanism can be resulted from the effective electrostatic interactions between the surface functional groups of BNQDs (denoted as amino) and target molecules (Xing et al., 2018). The electroactive surface areas of bare GCE, 2D-hBN/GCE and BNQDs/GCE were found to be 0.174 ± 0.03 cm^2, 0.551 ± 0.06 cm^2 and 1.365 ± 0.07 cm^2, respectively. The measurements were performed six times and the relative standard deviations (RSD) for bare GCE, 2D-hBN/GCE and BNQDs/GCE were calculated as 0.17%, 0.23% and 0.47%, respectively. The electroactive surface areas of the electrodes were obtained in the presence of 1.0 mM $[Fe(CN)_6]^{3-}$ solution containing 0.1 M KCl by the equation (Randles–Sevcik) of $i_p = 2.69 \times 10^5\ A\ n^{3/2}\ D^{1/2}\ C\ v^{1/2}$, where i_p was the current, C (mol cm^{-3}) was the concentration of $[Fe(CN)_6]^{3-}$, v was the scan rate (10–500 V s^{-1}) and A was standing for the surface area (cm^2) (n = 1, D = 7.6 × 10^{-6} cm^2 s^{-1} for $[Fe(CN)_6]^{3-}$) (Yola et al., 2016). The results were verified by EIS experiments. According to Fig. 2B, the values of charge transfer resistance (Rct) were found to be 150 Ω (curve c), 100 Ω (curve b) and 50 Ω (curve a). Hence, Rct values were consistent with CV results. A linear dependency was obtained between the anodic and

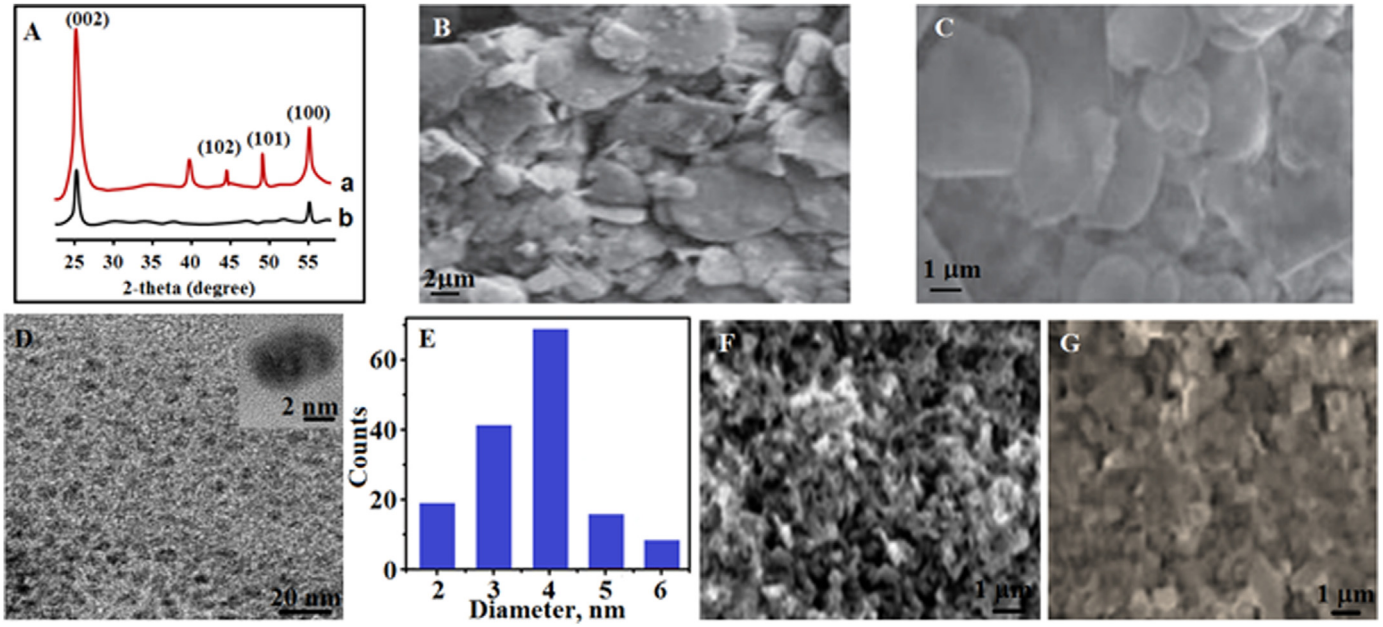

Fig. 1. XRD pattern (A) of bulk boron nitride (curve a) and 2D-hBN nanosheets (curve b); SEM images of (B) bulk boron nitride; (C) 2D-hBN nanosheets; (D) TEM image of BNQDs; (E) Size distributions of BNQDs; SEM images of (F) MIP/BNQDs/GCE; (G) NIP/BNQDs/GCE.

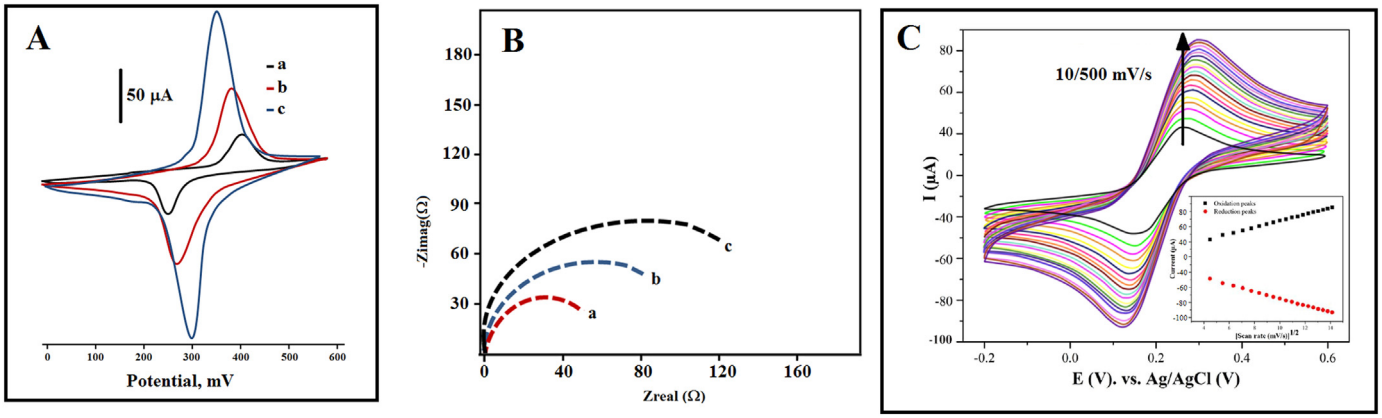

Fig. 2. (A) Cyclic voltammograms at (a) bare GCE, (b) 2D-hBN/GCE, (c) BNQDs/GCE; (B) EIS response at (a) BNQDs/GCE, (b) 2D-hBN/GCE, (c) bare GCE; Redox probe: 1.0 mM $[Fe(CN)_6]^{3-}$ containing 0.1 M KCl, Scan rate: 100 mV s^{-1}; (C) Cyclic voltammograms of the developed imprinting electrode (MIP/BNQDs/GCE) at different scan rates (10–500 mV s^{-1}). Inset is effect of different scan rate on the cathodic and anodic currents as a function of square root of the scan rate.

cathodic peak signals and the square root of the scan rate over the range of 10–500 mV s^{-1} (Fig. 2C), indicating that the developed biosensor interface (MIP/BNQDs/GCE) had diffusion controlled. The following linear regression equations were presented below:

$$Ipa = 4.4678(v)^{1/2} + 4.1937 (R^2 = 0.9996)$$

$$Ipc = -4.5179(v)^{1/2} - 7.8130 (R^2 = 0.9994)$$

In addition, when the scan rate was increased, the anodic and cathodic potentials shifted to positive and negative potentials, respectively. This situation revealed typical quasi-reversible electron transfer kinetics on MIP/BNQDs/GCE.

3.3. Formation of cTnI imprinted electrode on BNQDs

The oxidation potential of 100.0 mM pyrrole containing 25.0 mM cTnI in 0.1 M PBS was 0.75 V on first scan (scan rate: 100 mV s^{-1}, initial potential: +0.0 V and final potential: +1.0 V) (Fig. 3A). It was observed that the current signal with irreversible peak at 0.75 V slowly diminished with subsequent scans. They disappeared at the 10th cycle on BNQDs/GCE. Hence, cTnI imprinted electrode was successfully formed on BNQDs/GCE.

The curve a of Fig. 3B was corresponded to the signal of MIP/BNQDs/GCE without template in 0.1 M PBS (pH 7.0). Hence, the obvious signal response was not observed due to the blank solution. However, the MIP/BNQDs/GCE demonstrated an obvious current signal at + 0.20 V against 5.0 ng mL^{-1} cTnI (curve c of Fig. 3B). NIP/BNQDs/GCE was also prepared without cTnI analyte. The small signal was observed in curve b of Fig. 3B. The different imprinted electrodes (MIP/BNQDs/GCE, MIP/2D-hBN/GCE, MIP/GCE) were also prepared (Fig. 3C). According to Fig. 3C, the MIP/BNQDs/GCE (curve a) indicated the most signal increase in comparison with other imprinted electrodes.

3.4. Optimization studies

3.4.1. The pH effect

The pH is an important factor in terms of the electrochemical behavior of a developed biosensor and activity of cTnI in real sample medium. According to DPV signals of cTnI in the range of pH 5.0–9.0, they increased up to pH 7.0 (Fig. S1A). After pH 7.0, the signals diminished or remained constant. Thus, pH 7.0 was selected as the optimum pH for subsequent experiments (Rezaei et al., 2018).

3.4.2. The mole ratio template molecule to monomer effect

The mole ratio (cTnI/pyrrole) effect was investigated in a range of 1:2–1:6 (Fig. S1B). It was noted that the signals of DPVs up to 100.0 mM pyrrole increased significantly. The crucial increase on signals of DPVs resulted from the increase of binding site. Nonetheless, if the quantity of pyrrole increased further, the thicker polymer would be emerged on BNQDs/GCE. On the other hand, non-specific interactions on electrode surface occurred and finally, the optimum mole ratio was found as 1:4 in the study.

3.4.3. The desorption (removal of cTnI from electrode surface) time effect

The signals of DPVs increased until 15. minute (Fig. S1C). After desorption time of 15 min in bath (25 mL, 1.0 M NaCl solution, 200 rpm) at room temperature, they remained constant. Thus, it could be highlighted that no cTnI molecule was found on MIP/BNQDs/GCE and the removal of cTnI molecule was completed.

3.4.4. The scan cycle effect

Five different cTnI imprinted electrodes were prepared by different CV scans (5, 10, 15, 20) (Fig. S1D) in this study. According to the signals of DPVs, the optimum and the highest signals were observed at the 10th scan cycle. It could be interpreted as a thicker cTnI imprinted polymer was observed on BNQDs/GCE after the 10th scan cycle. This situation indicated the difficult removal of cTnI molecules on electrode surface. Thus, the 10th scan cycle was selected as optimum scan for subsequent experiments (Parameters: scan rate: 100 mV s^{-1}, initial potential: +0.0 V and final potential: +1.0 V).

3.5. Linearity range

Fig. 4 indicated the relation between current signals and cTnI concentrations at MIP/BNQDs/GCE (from 0.01 ng mL^{-1} to 5.00 ng mL^{-1}). The regression equations were as y (µA) = 10.028 × (nM) - 0.1124 for MIP and y (µA) = 1.2234 × (nM) - 0.2069 for NIP. Thus, this study has shown that MIP electrode was found to be more sensitivity to cTnI analyte. (Inset of Fig. 4). It was related to the basic adsorption phenomena describing concentration difference between liquid and solid phases on MIP electrode. These phases drive cTnI through the electrode surface to interact with specific ligands/cavities. The quantification limit (LOQ) and LOD for cTnI were obtained as 0.01 ng mL^{-1} and 0.0005 ng mL^{-1}, respectively. Moreover, Table 1 presented the comparisons between the MIP sensor and other systems. We have showed the significant advantages of the proposed method in this study. The molecular imprinted electrochemical biosensor with high selectivity was prepared. The obtained selectivity was found to be better in comparison with other systems briefly stated in Table 1. On the other hand, the nanomaterial was also prepared under solvothermal conditions in this study. According to the findings, the minimal waste formation in

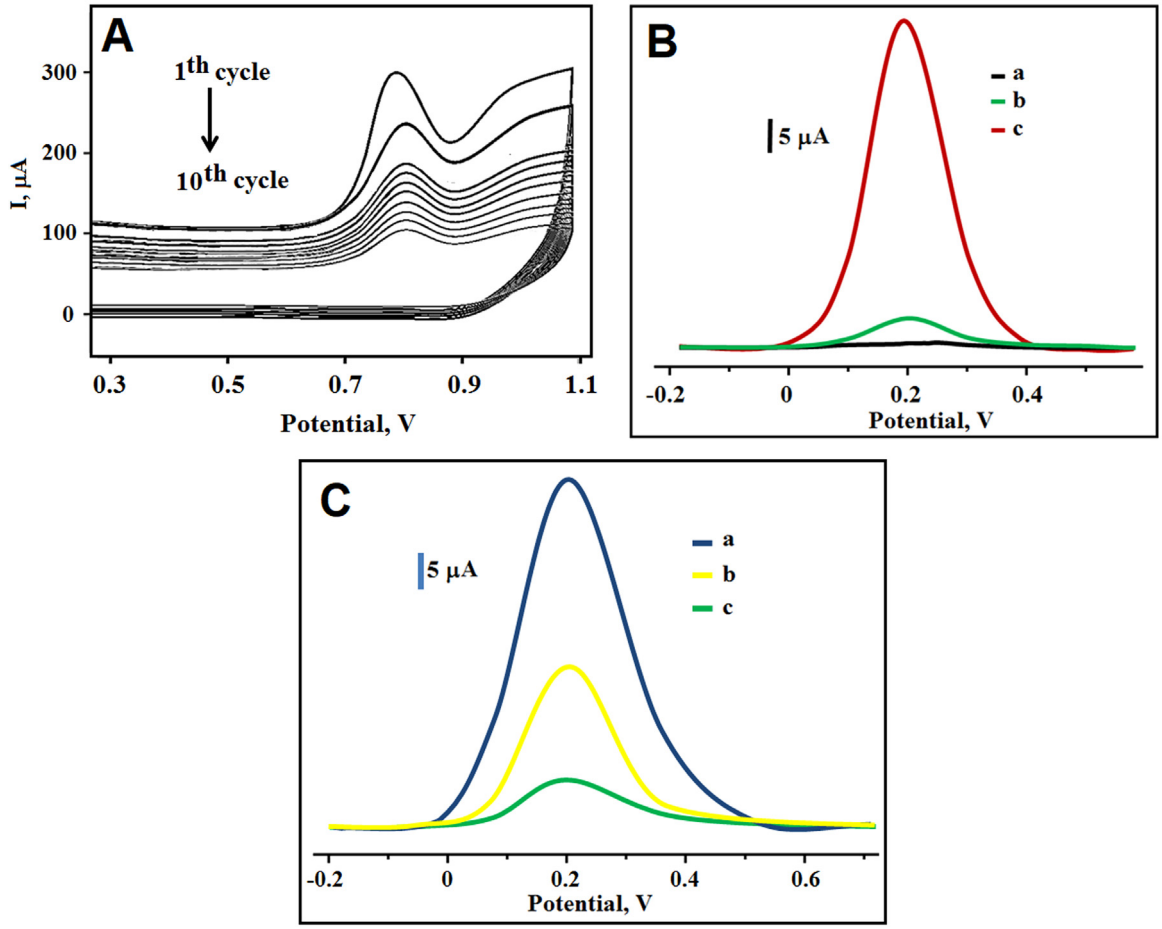

Fig. 3. (A) The polymerization of 100 mM pyrrole containing 25.0 mM cTnI on BNQDs/GCE (Scan rate: 100 mV s^{-1}); (B) The differential pulse voltammograms (DPVs) of the prepared electrodes in this study: (a) MIP/BNQDs/GCE in blank buffer solution, (b) NIP/BNQDs/GCE after rebinding of 5.0 ng mL^{-1} cTnI, (c) MIP/BNQDs/GCE after rebinding of 5.0 ng mL^{-1} cTnI (frequency of 50 Hz, pulse amplitude of 20 mV, scan increment of 3 mV) (C) DPVs of different molecular imprinted electrodes after rebinding of 5.0 ng mL^{-1} cTnI (a) BNQDs/GCE; (b) 2D-hBN/GCE; (c) bare GCE (frequency of 50 Hz, pulse amplitude of 20 mV, scan increment of 3 mV).

preparation of boron nitride quantum dots was obtained. Moreover, cheaper, eco-friendly and highly efficient nanomaterial was also found in comparison with multi-walled carbon nanotubes, carbon nanofiber, gold nanoparticles-graphene, gold nanoparticles and platinum nanoparticles. The processes of synthesis, purification, fabrication and functionalization of these nanomaterials were also required some special treatments, skills and time. Immunochromatographic (Penttilä et al., 1999), fluorescence (Seo et al., 2016) and surface plasmon resonance (SPR) (Dutra and Kubota, 2007) methods were developed for the determination of human cardiac troponin. However, there were various negative factors such as material consumption, complexity and high cost of these methods. Finally, MIP/BNQDs/GCE (LOD: 0.0005 ng mL^{-1}) was found to reveal higher sensitivity in comparison with other analytical methods.

3.6. Recovery

It was highlighted in Table S1 that, the developed biosensor was found to have a high selectivity due to the close values to 100.00%. In addition, standard addition method was applied to cTnI free plasma samples. The calibration equation was as y (µA) = 10.819 × (nM) + 1.9634 for MIP/BNQDs/GCE. On the other hand, no significance difference between the slopes of regression equations of linear calibration technique and standard addition method was found. According to the recovery results and standard addition method, the matrix in plasma sample had no effect on selective detection of cTnI by using MIP/BNQDs/GCE. Subsequently, the selective determination of cTnI in plasma samples can be completed successfully on MIP/BNQDs/GCE. Consequently, the matrix presence in plasma sample had no significant effect on the selective analysis of cTnI.

A rapid, simple and sensitive LC–MS/MS method was used in order to evaluate the validity of the developed electrode (Berna et al., 2007). Table S2 presented the results obtained by the two different methods for the determination of cTnI in human plasma samples. These results were compared by Wilcoxon test and no significant difference was found between the obtained results of MIP/BNQDs/GCE and LC–MS/MS ($T_{calculated} > T_{tabulated}$, $p > 0.05$).

3.7. Selectivity, stability, repeatability, reproducibility and reusability of MIP/BNQDs/GCE

The selectivity tests were performed by preparing four different solutions. The contents of the solutions were stated below:

Solution (1): only 5.0 ng mL^{-1} cTnI in 0.1 M PBS (pH 7.0)
Solution (2): only 5.0 ng mL^{-1} MYG in 0.1 M PBS (pH 7.0)
Solution (3): only 5.0 ng mL^{-1} BSA in 0.1 M PBS (pH 7.0)
Solution (4): only 5.0 ng mL^{-1} cTnT in 0.1 M PBS (pH 7.0)

The cTnI imprinted electrode (MIP) was separately interacted with each of the solutions. The obtained voltammograms were shown on Fig. S2A. The highest peak signals (ΔI = 50.00 µA) were normally obtained

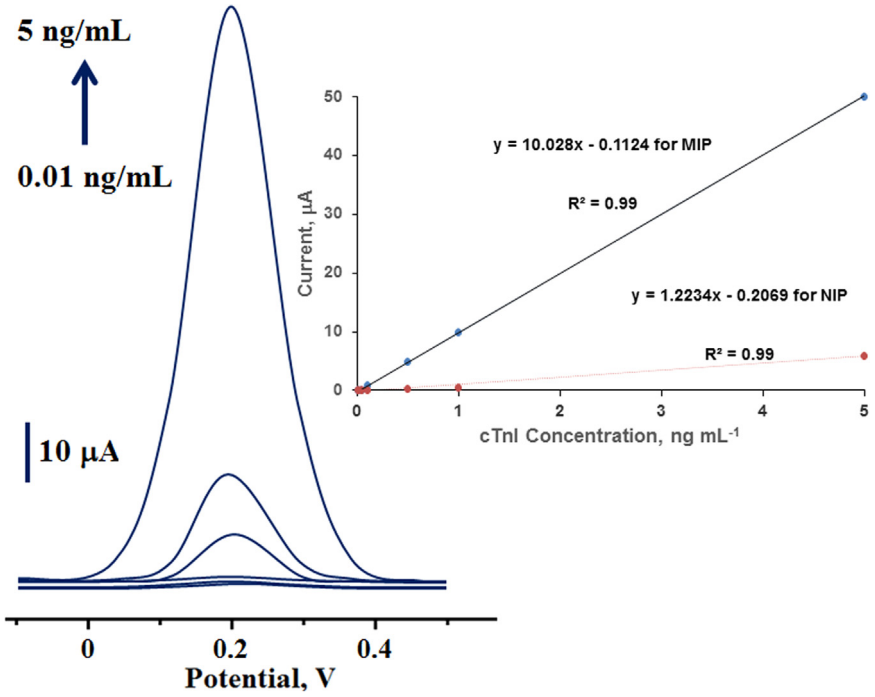

Fig. 4. DPVs with different cTnI concentrations at MIP/BNQDs/GCE in pH 7.0 of PBS (from 0.01 ng mL^{-1} to 5.00 ng mL^{-1} cTnI) (frequency of 50 Hz, pulse amplitude of 20 mV, scan increment of 3 mV): Inset: Calibration curve of cTnI for MIP and NIP electrodes.

Table 1
Comparison of the biosensor in this study with other methods.

Material or Method	Linear Range (ng mL^{-1})	LOD (ng mL^{-1})	Ref.
CMWCNT-WNFs	0.5–100.0	0.04	(Rezaei et al., 2018)
G-MWCNT/PtNPs	0.001–10.0	0.001	(Singal et al., 2016)
PDMS-AuNPs	0.01–50.0	0.004	(Zhou et al., 2010)
PDMS	0.2–1000.0	0.148	(Ko et al., 2007)
AuNPs/Gr	0.05–3.0	0.05	(Liu et al., 2016)
cAu	0.5–5.0	0.20	(Guo et al., 2005)
CTS-AuNPs	0.1–31.5	1.10	(Brondani et al., 2014)
Pt NPs-Gr	0.0025–10	0.04	(Singal et al., 2014)
CNF	0.25–1.0	0.20	(Periyakaruppan et al., 2013)
MIP/BNQDs/GCE	***0.01–5.00***	***0.0005***	***This study***

CMWCNT-WNFs: carboxylated multi-walled carbon nanotube-embedded whiskered nanofibers; G-MWCNT/PtNPs: graphene and multiwalled carbon nanotubes and decorated with platinum nanoparticles; PDMS-AuNPs: poly (dimethylsiloxane)-gold nanoparticles; PDMS: poly(dimethylsiloxane); AuNPs/Gr: gold nanoparticles-graphene; cAu: Colloidal gold; CTS-AuNPs: chitosan-stabilized gold nanoparticles; Pt NPs-Gr: Pt nanoparticles-graphene; CNF: carbon nanofiber.

in the presence of 5.0 ng mL^{-1} cTnI (solution:1 only) by using cTnI imprinted electrode. It was noted that cTnI imprinted electrode revealed low non-specific responses for MYG (ΔI = 10.00 µA), BSA (ΔI = 5.00 µA) and cTnT (ΔI = 2.50 µA). These responses were due to structural and physico-chemical similarities between cTnI and the other interfering proteins (MYG, BSA and cTnT). In Fig. S2A, it was highlighted that MIP/BNQDs/GCE was found to be 5.0, 10.0 and 20.0 times selective in terms of cTnI in comparison with MYG, BSA and cTnT (Table S3). Therefore, we could reach the conclusion that the molecular imprinting technique provided high selectivity for cTnI detection. cTnI non-imprinted BNQDs/GCE (NIP) was also prepared to display the specificity of cTnI imprinted electrode and the signals of nonimprinted electrode against Solution (1), Solution (2), Solution (3) and Solution (4) were found as 3.50, 3.00, 2.00 and 1.00, respectively (Fig. S2B). The selectivity coefficients for cTnI non-imprinted BNQDs/GCE in respect to MYG, BSA and cTnT were calculated as 1.17, 1.75 and 3.50, respectively. The relative selectivity constants showing the selectivity display that cTnI imprinted electrode was 4.27, 5.71 and 5.71 times more selective in comparison with MYG, BSA and cTnT, respectively.

For the stability of MIP/BNQDs/GCE, the signals of 5.0 ng mL^{-1} cTnI on MIP/BNQDs/GCE were measured during 60 days and the repeated signals (about 50.0 µA with 0.62% of relative standard deviation) were obtained. After each measurement, the electrodes were regenerated in order to put them into desorption agent (25 mL, 1.0 M NaCl solution) between the measurements. According to the results shown in Fig. S3, the imprinted biosensor was found to have a good stability.

For repeatability test of MIP/BNQDs/GCE in the presence of 5.0 ng mL^{-1} cTnI, 50 differential pulse voltammograms were taken and the repeated signals (relative standard deviation was 0.83%) were obtained.

The reproducibility test was performed with ten different MIP/BNQDs modified glassy carbon electrodes. These imprinted electrodes were fabricated independently by using the same procedure. The relative standard deviation value was found to 0.17% for current signal in the presence of 5.0 ng mL^{-1} cTnI and it indicated the reliability of biosensor preparation procedure.

Finally, the reusability of MIP/BNQDs/GCE was examined. According to the results, MIP/BNQDs/GCE was not found as a disposable sensor. It could be used at least 25 times (relative standard deviation was 0.23%) after washing with 0.1 M PBS (pH 7.0).

4. Conclusion

In the present study, we have combined the advantages of boron nitride quantum dots and molecular imprinting for detection of cardiac Troponin-I. Therefore, cardiac Troponin-I has been imprinted on polymeric films on the glassy carbon electrode by means of a molecular imprinting approach. Hence, the more specific cavities in the polymeric matrices were formed for cardiac Troponin-I in comparison with NIP. The prepared nanomaterials were firstly characterized by TEM, SEM, XRD, CV and EIS. According to the characterization studies, the

obtained BNQDs were well dispersed with uniform lateral sizes and the average lateral sizes were found to be 4.4 ± 0.6 nm. The linearity range (0.01–5.00 ng mL^{-1}), LOQ (0.01 ng mL^{-1}) and LOD (0.0005 ng mL^{-1}) values were calculated for proposed biosensor. According to the recovery experiments and standard addition technique, it could be stated that the matrix presence in plasma sample had no effect on the selective analysis of cardiac Troponin-I. In addition, the developed biosensor was found to be stable, repeatable, reusable and selective. Finally, the prepared biosensor showed high selectivity and sensitivity in plasma samples in comparison with other analytical methods.

Appendix A. Supporting information

Supplementary data associated with this article can be found in the online version at doi:10.1016/j.bios.2018.11.016.

References

Apple, F.S., Falahati, A., Paulsen, P.R., Miller, E.A., Sharkey, S.W., 1997. Clin. Chem. 43 (11), 2047–2051.
Atar, N., Yola, M.L., 2018. J. Electrochem. Soc. 165 (5), H255–H262.
Berna, M.J., Zhen, Y., Watson, D.E., Hale, J.E., Ackermann, B.L., 2007. Anal. Chem. 79 (11), 4199–4205.
Beytur, M., Kardaş, F., Akyıldırım, O., Özkan, A., Bankoğlu, B., Yüksek, H., Yola, M.L., Atar, N., 2018. J. Mol. Liq. 251, 212–217.
Boriani, G., Biffi, M., Cervi, V., Bronzetti, G., Magagnoli, G., Zannoli, R., Branzi, A., 2000. Chest 118 (2), 342–347.
Brondani, D., Piovesan, J.V., Westphal, E., Gallardo, H., Fireman Dutra, R.A., Spinelli, A., Vieira, I.C., 2014. Analyst 139 (20), 5200–5208.
Cho, I.-H., Paek, E.-H., Kim, Y.-K., Kim, J.-H., Paek, S.-H., 2009. Anal. Chim. Acta 632 (2), 247–255.
de Antonio, M., Lupón, J., Galán, A., Vila, J., Zamora, E., Urrutia, A., Díez, C., Coll, R., Altimir, S., Bayes-Genis, A., 2013. Clin. Chim. Acta 426, 18–24.
Dutra, R.F., Kubota, L.T., 2007. Clin. Chim. Acta 376 (1), 114–120.
Fredericks, S., Merton, G., Lerena, M.-J., Holt, D.W., 1998. Clin. Chem. 44 (2), 362–365.
Friess, U., Stark, M., 2009. Cardiac markers: a clear cause for point-of-care testing. Anal. Bioanal. Chem. 393 (5), 1453–1462.
Guo, H., He, N., Ge, S., Yang, D., Zhang, J., 2005. Microporous Mesoporous Mater. 85 (1), 89–95.
Hassan, J.J., Mahdi, M.A., Kasim, S.J., Ahmed, N.M., Abu Hassan, H., Hassan, Z., 2012. Appl. Phys. Lett. 101 (26).
Hongling, L., Yingjie, T.R., Hon, T.S., Xu, Z., Tong, T.E.H., 2015. Small 11 (48), 6491–6499.
Ide, Y., Liu, F., Zhang, J., Kawamoto, N., Komaguchi, K., Bando, Y., Golberg, D., 2014. J. Mater. Chem. A 2 (12), 4150–4156.
Iwanaga, Y., Miyazaki, S., 2010. Circ. J. 74 (7), 1274–1282.
Khan, A.F., Brownson, D.A.C., Randviir, E.P., Smith, G.C., Banks, C.E., 2016. Anal. Chem. 88 (19), 9729–9737.
Ko, S., Kim, B., Jo, S.-S., Oh, S.Y., Park, J.-K., 2007. Biosens. Bioelectron. 23 (1), 51–59.
Lei, Z., Xu, S., Wan, J., Wu, P., 2015. Nanoscale 7 (45), 18902–18907.
Li, L.H., Chen, Y., Behan, G., Zhang, H., Petravic, M., Glushenkov, A.M., 2011. J. Mater. Chem. 21 (32), 11862–11866.
Liu, G., Qi, M., Zhang, Y., Cao, C., Goldys, E.M., 2016. Anal. Chim. Acta 909, 1–8.
Ramuz, M., Hama, A., Huerta, M., Rivnay, J., Leleux, P., Qwens, R.O., 2014. Adv. Mater. 26 (41), 7083–7090.
Mengli, L., Yuanhong, X., Yao, W., Xu, C., Xuqiang, J., Fushuang, N., Zhongqian, S., Jingquan, L., 2017. Adv. Opt. Mater. 5 (3), 1600661.
Penttilä, K., Koukkunen, H., Kemppainen, A., Halinen, M., Rantanen, T., Pyörälä, K., Penttilä, I., 1999. Int. J. Clin. Lab. Res. 29 (2), 93–101.
Periyakaruppan, A., Gandhiraman, R.P., Meyyappan, M., Koehne, J.E., 2013. Anal. Chem. 85 (8), 3858–3863.
Rezaei, B., Shoushtari, A.M., Rabiee, M., Uzun, L., Mak, W.C., Turner, A.P.F., 2018. Talanta 182, 178–186.
Seo, S.-M., Kim, S.-W., Park, J.-N., Cho, J.-H., Kim, H.-S., Paek, S.-H., 2016. Biosens. Bioelectron. 83, 19–26.
Singal, S., Srivastava, A.K., Biradar, A.M., Rajesh, Mulchandani A., 2014. Sens. Actuators, B 205, 363–370.
Singal, S., Srivastava, A.K., Gahtori, B., Rajesh, 2016. Microchim. Acta 183 (4), 1375–1384.
Weng, Q., Wang, B., Wang, X., Hanagata, N., Li, X., Liu, D., Wang, X., Jiang, X., Bando, Y., Golberg, D., 2014. ACS Nano 8 (6), 6123–6130.
Xing, H., Zhai, Q., Zhang, X., Li, J., Wang, E., 2018. Anal. Chem. 90 (3), 2141–2147.
Yola, M.L., Atar, N., 2017a. Ind. Eng. Chem. Res. 56 (27), 7631–7639.
Yola, M.L., Atar, N., 2017b. J. Electrochem. Soc. 164 (6), B223–B229.
Yola, M.L., Göde, C., Atar, N., 2017. Electrochim. Acta 246, 135–140.
Yola, M.L., Eren, T., Atar, N., Saral, H., Ermis, İ., 2016. Electroanalysis 28 (3), 570–579.
Zhou, F., Lu, M., Wang, W., Bian, Z.-P., Zhang, J.-R., Zhu, J.-J., 2010. Clin. Chem. 56 (11), 1701–1707.